GEOPHYSICS, VOL. 67, NO. 1 (JANUARY–FEBRUARY 2002); P. 300–306, 8 FIGS.
10.1190/1.1451802

AVO and AVA inversion for fractured reservoir characterization

Matteo Mario Beretta*, Giancarlo Bernasconi*, and Giuseppe Drufuca*

ABSTRACT

Seismic wave reflection amplitudes are used to detect fluids and fracture properties in reservoirs. This paper studies the characterization of a vertically fractured fluid-filled reservoir by analyzing the reflection amplitudes of *P*-waves with varying incident and azimuthal angles. The reservoir is modeled as a horizontal transversely isotropic medium embedded in an isotropic background, and the linearized *P*-waves reflection coefficient are considered. The conditioning of the inverse problem is analyzed, and fracture density is found to be the best conditioned parameter. Using diffraction tomography under the Born approximation, an inversion procedure is proposed in the transformed k–ω domain to detect fracture density variations within the reservoir. Seismic data are rearranged in pairs of incident and reflected plane waves, enlightening only one spectral component of the fracture density field at a time. Only the observable spectral components are inverted. Moreover, working in the transformed domain, picking reflection amplitudes is not required. An example of the inversion applied to a synthetic data set is presented. The limitation of source and receiver numbers and the finite bandwidth of the wavelet produce a loss of resolution, but the overall fracture density variations are recovered correctly.

INTRODUCTION

A large portion of the world's proven oil and gas reserves have been found in reservoir rocks that are naturally fractured. This explains the recent increasing interest in new techniques to improve the development and management of this kind of reservoir.

The amount of recoverable hydrocarbons depends on a number of factors, including interstitial porosity; pore size, shape, and interconnectivity; saturation of oil, gas, and water (Nelson, 1985); and fracture spacing, width, and orientation. In particular, knowing the fracture density variation between zones within a reservoir can help determine the location of the well.

It has become practical to use *P*-waves to detect fracture-induced azimuthal anisotropy (MacBeth and Lynn, 2000). The approach shifts the emphasis from the acquisition effort to additional processing, relying upon the detection of amplitude variations in individual prestack common reflection point (CRP), common depth point (CDP), and common midpoint (CMP) gathers. According to theory, the reflection coefficient contains combinations of the fracture's response to normal and tangential stress when the waves are incident at oblique angles. The additional dependency on the normal stress boundary condition provides the means to improve fracture determination. Such fracture-related anisotropy can be observed as a direction-dependent modification of the isotropic amplitude versus offset (AVO) variation (Lynn et al. 1996; Grimm et al., 1999; Lynn et al., 1999).

Using diffraction tomography theory and generalizing the technique presented in Bernasconi et al. (1997), we have developed a linearized inversion methodology in the k–ω domain that detects fracture density variation within a reservoir using *P*-wave reflection data. We consider small perturbations of a uniform isotropic background resulting from the presence of fluid-filled fractures. Seismic data are rearranged in plane waves: in the Born approximation each pair of incident and reflected plane waves enlightens only one spectral component of the fracture density field, which is inverted.

The method has the advantage of not requiring reflection amplitude picks.

THE INVERSE PROBLEM CONDITIONING

We use the horizonal transverse isotropy (HTI) model as an effective medium for vertically fractured rock, considered as a solid with weak distribution of parallel penny-shaped cracks (Hudson, 1980, 1981; Schoenberg, 1983; Schoenberg and Sayers, 1995). Under the hypothesis of small contrast interface (Zillmer et al., 1998, Rüger, 1997), we write the linearized *P*-wave reflection coefficient from the boundary between isotropic and vertically fractured media, with varying fracture density and filling-material properties (Beretta et al., 2000), as

Manuscript received by the Editor June 6, 2000; revised manuscript received March 27, 2001.
*Politecnico di Milano, Dipartimento di Elettronica e Informazione, Piazza Leonardo da Vinci 32, 20133 Milan, Italy. E-mail: beretta@elet.polimi.it; bernasco@elet.polimi.it; drufuca@elet.polimi.it.

$$R_{qPqP}(\theta,\phi) = \tilde{R}_{qPqP}(\theta,\phi) + \tilde{R}^{\epsilon}_{qPqP}(\theta,\phi)\frac{\Delta\epsilon}{\bar{\epsilon}} + \tilde{R}^{Z_P}_{qPqP}(\theta,\phi)\frac{\Delta Z_P}{\bar{Z}_P} + \tilde{R}^{Z_S}_{qPqP}(\theta,\phi)\frac{\Delta Z_S}{\bar{Z}_S}, \quad (1)$$

where ϵ is the fracture density, θ is the incidence angle, and ϕ is the azimuthal angle, and where $Z_P = \rho V_P^2$ and $Z_S = \rho V_S^2$ describe the isotropic fracture-filling material. The variables ϵ, Z_P, and Z_S define the parameter (model) space. The barred quantities represent the mean values, and the Δ quantities are the variations with respect to the mean values. The ˜ terms are the linearization coefficients.

We investigated the conditioning of the linearized inversion of P-wave reflection amplitudes, for either AVO or AVA acquisition, computing the singular value decomposition (SVD) of the relation between reflection amplitude and parameters [equation (1)], with respect of the maximum incident or azimuthal observation angle (Beretta et al., 2000). This allows a simple interpretation of the information contained in the reflections. We obtain orthogonal basis (eigenvectors) in the parameter (model) space and in the data space, linked by a diagonal matrix of eigenvalues. The eigenvalues represent the reflected energy from perturbations along the eigenvectors in the model space. If the orders of magnitude of the eigenvalues are very different from each other, then a high S/N ratio is needed to estimate the signal in the low-energy directions. The result (Beretta et al., 2000) is that the eigenvectors in the model space are almost parallel to the axes of the parameter space $[\Delta\epsilon/\bar{\epsilon},\ \Delta Z_P/\bar{Z}_P,\ \Delta Z_S/\bar{Z}_S]$ and that fracture density is the best conditioned parameter (Figures 1 and 2).

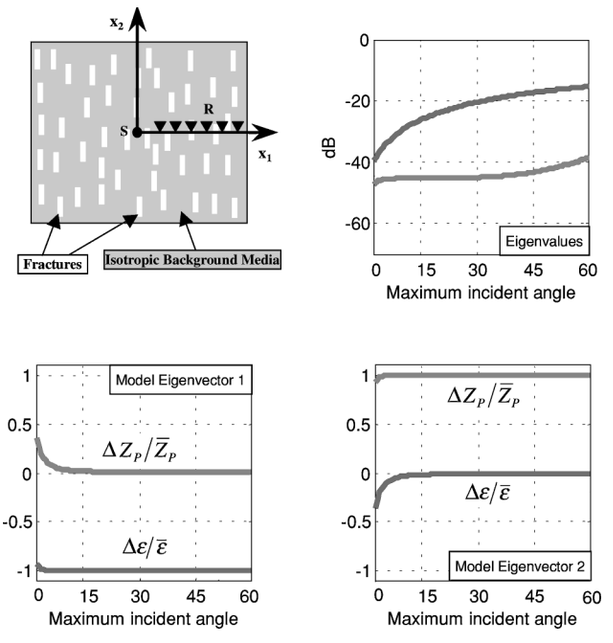

FIG. 1. AVO acquisition perpendicular to the fracture strike plane. Eigenvalues and eigenvectors of the linearized reflection coefficient in the model (parameter) space versus maximum incident angle. The minimum difference between the two eigenvalues is about 20 dB. The first eigenvector is related to fracture density ϵ.

REFLECTION COEFFICIENT FOR A SINUSOIDAL MEDIUM

We want to apply the diffraction tomography technique to the linearized inversion of reflection amplitudes. It is therefore mandatory to cast the problem in the transformed domain.

An inhomogeneous medium can be decomposed, by means of the 3-D Fourier transform, in its spectral components. A point of the medium spectrum, defined by the wavenumber $\mathbf{k}_m = [k_{mx}, k_{my}, k_{mz}]$, represents in the spatial domain a 1-D sinusoidal perturbation with a given period and direction. In this section, following De Nicolao et al. (1993), we derive the reflection coefficient for a sinusoidal component of a fractured medium.

Equation (1) can be written for a single interface as

$$\Delta R_{qPqP}(\theta,\phi) = R_{qPqP}(\theta,\phi) - \tilde{R}_{qPqP}(\theta,\phi) = \mathbf{a}_{qPqP}(\theta,\phi)\mathbf{m}, \quad (2)$$

where

$$\mathbf{a}_{qPqP}(\theta,\phi) = \left[\tilde{R}^{\epsilon}_{qPqP}(\theta,\phi),\ \tilde{R}^{Z_P}_{qPqP}(\theta,\phi),\ \tilde{R}^{Z_S}_{qPqP}(\theta,\phi)\right] \quad (3)$$

and

$$\mathbf{m} = \left[\frac{\Delta\epsilon}{\bar{\epsilon}},\ \frac{\Delta Z_P}{\bar{Z}_P},\ \frac{\Delta Z_S}{\bar{Z}_S}\right]^T.$$

If the fracture parameters are continuous functions $\mathbf{m}(\mathbf{r})$ of the position vector $\mathbf{r} = [x, y, z]$, the medium can be decomposed in a sequence of interfaces with infinitesimal thickness $d\mathbf{r}$. The

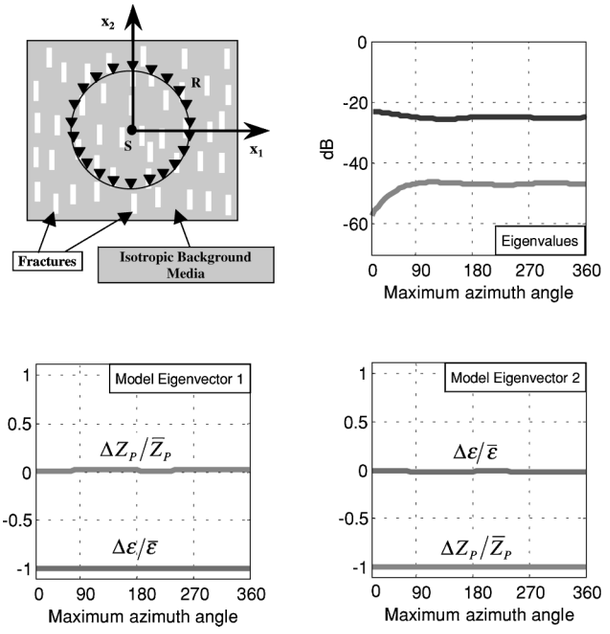

FIG. 2. AVA acquisition with 360° in azimuth (incident angle 35°). Azimuth angle is measured from the x_1 axis. Eigenvalues and eigenvectors of the linearized reflection coefficient in the model (parameter) space versus maximum azimuth angle. The minimum difference between the two eigenvalues is about 35 dB. The first eigenvector is related to fracture density ϵ. Moreover, as it can be concluded also from the forward problem, azimuth ranges >90° do not add more information.

linearized reflection coefficient for an infinitesimal thickness can be written as

$$\frac{\partial \Delta R_{qPqP}(\theta,\phi)}{\partial \mathbf{r}} \cdot d\mathbf{r} = \mathbf{a}_{qPqP}(\theta,\phi)\left[\frac{\partial \mathbf{m}(\mathbf{r})}{\partial \mathbf{r}} \cdot d\mathbf{r}\right] \quad (4)$$

and

$$\mathbf{m}(\mathbf{r}) = \left[\frac{\Delta\epsilon(\mathbf{r})}{\bar{\epsilon}}, \frac{\Delta Z_P(\mathbf{r})}{\bar{Z}_P}, \frac{\Delta Z_S(\mathbf{r})}{\bar{Z}_S}\right]^T. \quad (5)$$

By means of a Fourier transform, it is possible to decompose the perturbations in sums of sinusoids

$$\begin{aligned}
\frac{\Delta\hat{\epsilon}(\mathbf{k}_m)}{\bar{\epsilon}} &= \int_{-\infty}^{+\infty} \frac{\Delta\epsilon(\mathbf{r})}{\bar{\epsilon}} e^{i\mathbf{k}_m\cdot\mathbf{r}}\, d\mathbf{r},\\
\frac{\Delta\hat{Z}_P(\mathbf{k}_m)}{\bar{Z}_P} &= \int_{-\infty}^{+\infty} \frac{\Delta Z_P(\mathbf{r})}{\bar{Z}_P} e^{i\mathbf{k}_m\cdot\mathbf{r}}\, d\mathbf{r}, \quad (6)\\
\frac{\Delta\hat{Z}_S(\mathbf{k}_m)}{\bar{Z}_S} &= \int_{-\infty}^{+\infty} \frac{\Delta Z_S(\mathbf{r})}{\bar{Z}_S} e^{i\mathbf{k}_m\cdot\mathbf{r}}\, d\mathbf{r},
\end{aligned}$$

and

$$\begin{aligned}
\hat{\mathbf{m}}(\mathbf{k}_m) &= \left[\hat{m}_\epsilon(\mathbf{k}_m), \hat{m}_{Z_P}(\mathbf{k}_m), \hat{m}_{Z_S}(\mathbf{k}_m)\right]^T\\
&= \left[\frac{\Delta\hat{\epsilon}(\mathbf{k}_m)}{\bar{\epsilon}}, \frac{\Delta\hat{Z}_P(\mathbf{k}_m)}{\bar{Z}_P}, \frac{\Delta\hat{Z}_S(\mathbf{k}_m)}{\bar{Z}_S}\right]^T. \quad (7)
\end{aligned}$$

The $\hat{}$ indicates the Fourier transform. A single spectral component, identified by the wavenumber $\mathbf{k}_m$, corresponds to a sinusoidal 1-D perturbation in the space domain:

$$\mathbf{m}_{\mathbf{k}_m}(\mathbf{r}) = \hat{\mathbf{m}}(\mathbf{k}_m) e^{-i\mathbf{k}_m\cdot\mathbf{r}}. \quad (8)$$

From equations (4) and (8) it is possible to obtain the expression of the reflection coefficient for a sinusoidal perturbation with wavenumber $\mathbf{k}_m$:

$$\begin{aligned}
\frac{\partial \Delta R_{qPqP\mathbf{k}_m}}{\partial \mathbf{r}}(\theta,\phi,\mathbf{r}) &= \mathbf{a}_{qPqP}(\theta,\phi)\frac{\partial \mathbf{m}_{k_m}(\mathbf{r})}{\partial \mathbf{r}}\\
&= -i\,\mathbf{a}_{qPqP}(\theta,\phi)\hat{\mathbf{m}}(\mathbf{k}_m)\mathbf{k}_m e^{-i\mathbf{k}_m\cdot\mathbf{r}}.
\end{aligned} \quad (9)$$

By superposition, the response of an inhomogeneous medium is the sum of the responses of the single sinusoidal media:

$$\begin{aligned}
\frac{\partial \Delta R_{qPqP}(\theta,\phi,\mathbf{r})}{\partial \mathbf{r}} &= \mathbf{a}_{qPqP}(\theta,\phi)\frac{\partial \mathbf{m}(\mathbf{r})}{\partial \mathbf{r}}\\
&= -i\frac{1}{2\pi}\mathbf{a}_{qPqP}(\theta,\phi)\int_{-\infty}^{+\infty} \hat{\mathbf{m}}(\mathbf{k}_m)\mathbf{k}_m e^{-i\mathbf{k}_m\cdot\mathbf{r}}\, d\mathbf{k}_m. \quad (10)
\end{aligned}$$

The same approach can be applied to the other reflection coefficients, obtaining expressions similar to equation (10) with different values of $\mathbf{a}(\theta,\phi)$.

LINEARIZED INVERSION IN THE TRANSFORMED DOMAIN

The hypothesis of small contrasts enables us to use the Born approximation so that equation (9) is the starting point for a linearized inversion in the transformed wavenumber–frequency (k–ω) domain.

The input data are a set of common shot gathers. They form a hypercube (data space, Figure 3) whose axes are

$$\begin{aligned}
t &\Rightarrow \text{time},\\
\mathbf{r}_s = (x_s, y_s) &\Rightarrow \text{source position},\\
\mathbf{r}_g = (x_g, y_g) &\Rightarrow \text{geophone position}.
\end{aligned}$$

The Fourier transform of the data maps the $(t, \mathbf{r}_g, \mathbf{r}_s)$ domain into the $(\omega, \mathbf{k}_g, \mathbf{k}_s)$ domain, where

$$\begin{aligned}
\omega &\Rightarrow \text{angular frequency},\\
\mathbf{k}_s = (k_{sx}, k_{sy}) &\Rightarrow \text{source wavenumber},\\
\mathbf{k}_g = (k_{gx}, k_{gy}) &\Rightarrow \text{geophone wavenumber}.
\end{aligned}$$

The basic principle of diffraction tomography (Figure 4) states that a reflected monochromatic plane wave (wavenumber $\mathbf{k}_r$) resulting from an incident plane wave (wavenumber $\mathbf{k}_i$) relates to only one Fourier component of the medium (wavenumber $\mathbf{k}_m$):

$$\mathbf{k}_m = \mathbf{k}_r - \mathbf{k}_i. \quad (11)$$

The relations between incident and reflected wavenumbers in equation (11) and source and geophone wavenumbers are (Wu and Toksöz, 1987)

$$\begin{aligned}
\mathbf{k}_i &= -\mathbf{k}_s,\\
\mathbf{k}_r &= \mathbf{k}_g.
\end{aligned} \quad (12)$$

Substituting equation (12) in equation (11) reveals the mapping from data space $(\omega, \mathbf{k}_s, \mathbf{k}_g)$ to model space $(\mathbf{k}_m, \theta, \phi)$:

$$\begin{aligned}
k_{mx} &= k_{gx} + k_{sx},\\
k_{my} &= k_{gy} + k_{sy}, \quad (13)\\
k_{mz} &= \sqrt{\left(\frac{\omega}{v_i}\right)^2 - k_{sx}^2 - k_{sy}^2} + \sqrt{\left(\frac{\omega}{v_r}\right)^2 - k_{gx}^2 - k_{gy}^2},
\end{aligned}$$

where v_i and v_r are the velocities of the incident and the reflected wave, respectively. It is important to notice that a point

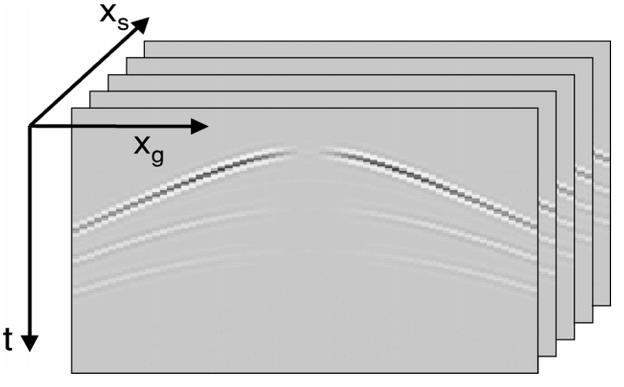

FIG. 3. An example of a 3-D data set cube (data space) for a 2-D acquisition profile. In this case x_s is the source position along the profile, x_g is the receiver (geophone) position, and t is time. For 3-D acquisition the data cube has five dimensions.

$(\omega, \mathbf{k}_s, \mathbf{k}_g)$ in the data space determines the angles θ and ϕ of the incident plane wave (Figure 4). The ω-dependence is transformed into incidence angle and azimuth dependence (see Appendices A and B for a detailed calculation):

$$\cos\theta = \frac{\left(\frac{\omega}{v_i}\right)^2 - \left(\frac{\omega}{v_r}\right)^2 + k_{mx}^2 + k_{my}^2 + k_{mz}^2}{2\left(\frac{\omega}{v_i}\right)\sqrt{k_{mx}^2 + k_{my}^2 + k_{mz}^2}},$$
$$\phi = \phi_{n_f} - \phi_{k_i}, \tag{14}$$

where

$$\phi_{n_f} = \arctan\left[\frac{\bar{n}_{fy}}{\bar{n}_{fx}}\right],$$
$$\phi_{k_i} = \arctan\left[\frac{\bar{k}_{iy}}{\bar{k}_{ix}}\right], \tag{15}$$

$\mathbf{n}_f$ is the normal to the fracture strike plane, and $(\bar{n}_{fx}, \bar{n}_{fy})$ and $(\bar{k}_{ix}, \bar{k}_{iy})$ are the components of $\mathbf{n}_f$ and the incident wavenumber vector $\mathbf{k}_i$ in the Γ plane (Figures 4 and B-1). For each point (k_{mx}, k_{my}, k_{mz}) in the transformed model domain (that is, for each sinusoidal component in the model space domain), the relation between recorded data and parameters with respect to the angles θ and ϕ is

$$\mathbf{d}(\theta, \phi) = \mathbf{A}_{qPqP}(\theta, \phi)\,\mathbf{m}, \tag{16}$$

where $\mathbf{d}(\theta, \phi)$ is the vector of the amplitude reflections, $\mathbf{m}$ describes the model perturbation, and the matrix $\mathbf{A}_{qPqP}$ contains the incident and azimuth angle dependence, the source spectrum, the propagation effects, and the directivity of source and receivers.

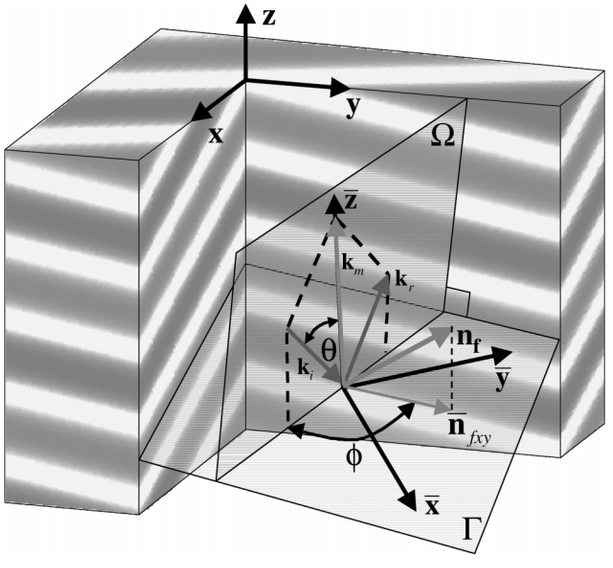

FIG. 4. Diffraction tomography. Relation between medium wavenumber $\mathbf{k_m}$, incident wavenumber $\mathbf{k_i}$, and reflected wavenumber $\mathbf{k_r}$. The gray density shading represents a 1-D sinusoidal perturbation with wavenumber $\mathbf{k_m}$. The plane Ω contains the incident vector $\mathbf{k_i}$, the medium vector $\mathbf{k_m}$, and the reflected vector $\mathbf{k_r}$. The plane Γ is perpendicular to $\mathbf{k_m}$; θ is the incident angle; and ϕ is the angle in plane Γ between the projection of the vector $\mathbf{k}_i$ and the normal to the fractures $\mathbf{n_f}$. The coordinate system $(\bar{x}, \bar{y}, \bar{z})$ has the vertical $\bar{z}$ axis in the direction of $\mathbf{k_m}$ and the plane $\bar{x}\bar{y}$ on the Γ plane.

In general $\mathbf{A}_{qPqP}$ is not square and poorly conditioned. For the inversion we use the SVD of the relation data parameters $\mathbf{A}_{qPqP} = \mathbf{U}\mathbf{\Lambda}\mathbf{V}^T$ (Lines and Treitel, 1984). The matrix $\mathbf{U}$ defines the eigenvectors in the data space. The symbol $\mathbf{\Lambda}$ is the diagonal matrix of singular values; they represent the energy in the data resulting from a unitary variation along the eigenvector axes in the model space. The term $\mathbf{V}$ contains the eigenvectors in the model space.

The model perturbation with wavenumber (k_{mx}, k_{my}, k_{mz}) can be obtained by inverting equation (16):

$$\mathbf{m} \cong \mathbf{V}\mathbf{\Lambda}^{-1}\mathbf{U}^T\mathbf{d}. \tag{17}$$

In practice we extract from the seismic data the reflections resulting from pairs of incident and reflected plane waves. Each of them relates to a single spectral component [equation (13)], incident angle, and azimuth angle [equations (14) and (15)] of the medium perturbation. At the end of this mapping procedure, for each spectral component we invert the angle dependence (elements of $\mathbf{d}$) to get the medium perturbation parameters $\mathbf{m}$ [equation (17)]. The final image is obtained by an inverse Fourier transform to the spatial (x, y, z) domain.

Because of the finite range of sources, receivers, frequency components, and observation angles, only part of the entire model spectrum can be recovered. Nonobservable components of the spectrum (null space) are not inverted.

The ill conditioning of the inverse problem (Beretta et al., 2000) does not allow a good estimate of all fracture parameters. Even small numerical errors can deteriorate the quality of the inversion and can produce interference between the estimated parameters. Similar effects result from the practical aspects of data collection and processing. Truncations resulting from the finite length of the cable and the finite number of sources produce aliasing and distortions in the reconstructed model. For these reasons, in the linearized approach we use qP–qP reflections to estimate only fracture density.

RESULTS

We are testing our inversion on synthetic data sets. We are able to invert small variations of density fractures on a uniform background: this suggests the application of the procedure to a limited area (target) where this condition can be verified. Moreover, we assume to collect reflection seismograms on the top of the target. In general this implies a datuming step prior to inversion, to bring sources and receivers from the original depth level to the target level (Wapenaar et al., 1989).

The model presented here is a homogeneous isotropic medium ($V_p = 5800$ m/s, $V_s = 3349$ m/s, $\rho = 2600$ kg/m^3) with some fluid-filled fractured zones. The filling material is water. Fracture density varies up to 10% (Figure 5a). The input data consist of 128 shot gathers on a 2-D seismic line recorded on top of the target zone. Source spacing is 30 m; receiver spacing is 25 m. Each shot has a split-spread geometry perpendicular to the fracture strike plane with 64 receivers.

The reference input model is a homogeneous vertically fractured medium with correct background isotropic parameters, fluid filling parameters, and constant density fracture of 10%. The output of the inversion is the map of density fracture variations.

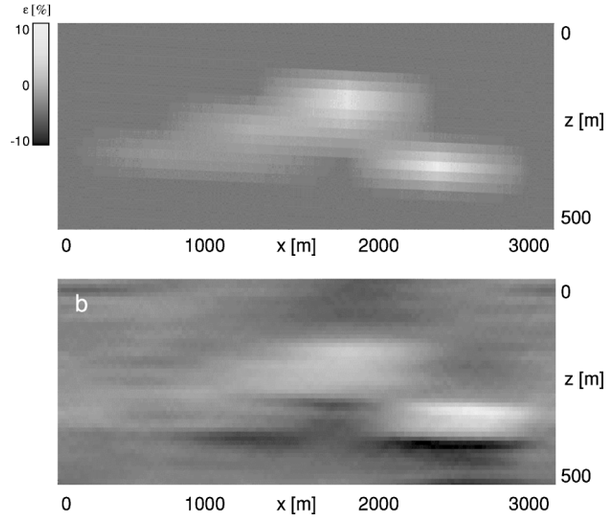

FIG. 5. Homogeneous isotropic medium ($V_P = 5800$ m/s, $V_S = 3349$ m/s, $\rho = 2600$ kg/m^3) with water-filled vertical fractures. Fracture density varies up to 10%. (a) Original model. (b) Inverted model.

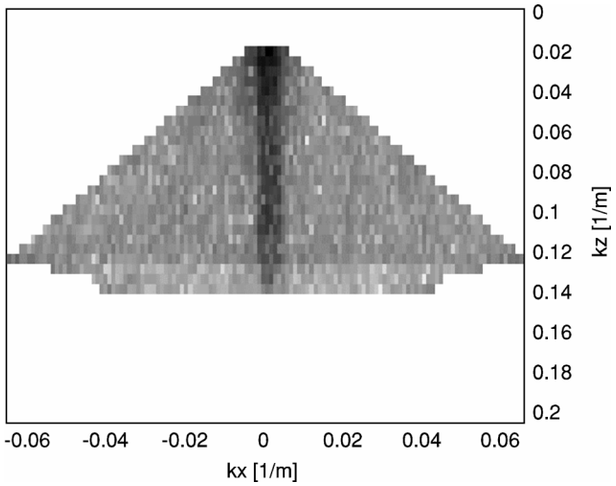

FIG. 6. Spectrum (absolute value) of the inverted model in Figure 5. Because of the finite range of sources, receivers, frequency components, and observation angles, only part of the entire model spectrum can be recovered. Nonobservable components (white background) are not inverted.

Figure 5 shows the original fracture density and the result of inversion; the position and the relative amplitudes of the anomalies are retrieved correctly.

Because the number of sources and receivers is finite, the observation angles are limited and the inverted image appears smoothed. In fact, Figure 6 shows the spectrum (absolute value) of the inverted image, which is built up only with the well-conditioned components. The angular limitation produces a truncation of the spectrum.

CONCLUSIONS

We have studied the characterization of a vertically fluid-filled fractured reservoir using the reflection amplitudes of *P*-waves with varying incident and azimuthal angle. We have shown that, in the linearized approach, the inverse problem is ill conditioned and only fracture density can be obtained reliably.

We have derived the linearized reflection coefficient for a 1-D sinusoidal medium, and we have presented a procedure to determine fracture density variations within the reservoir, based on a diffraction tomography technique. Seismic data are rearranged in plane waves; in the Born approximation each pair of incident and reflected plane waves enlightens only one spectral component of the fracture density field, which is inverted. Ambiguities are carefully avoided by inverting only well-conditioned components. Working in the transformed domain, we can control the effects of the limited angular coverage. Moreover, no picking of events is required.

We need reflection seismograms recorded on the top of the target zone. In general this requires an amplitude-preserving datuming step prior to the inversion.

The technique was tested successfully on a synthetic data set.

ACKNOWLEDGMENTS

We thank C. MacBeth for helpful suggestions. The synthetic seismograms have been computed with the program ANRAY 4.01 by D. Gajewski and I. Psencik (http://seis.karlov.mff.cuni.cz/software/sw3dcd1/anray/document/readme.htm).

REFERENCES

Beretta, M. M., Bernasconi, G., and Drufuca, G., 2000, Linearized inversion of vertically fractured media: Geophys. J. Internat., **143**, 965–968.

Bernasconi, G., Drufuca, G., and Rocca, F., 1997, Linearized target oriented inversion: Application to real data: J. Seis. Expl., **6**, 143–158.

De Nicolao, A., Drufuca, G., and Rocca, F., 1993, Eigenvalues and eigenvectors of linearized elastic inversion: Geophysics, **58**, 670–679.

Grimm, R. E., Lynn, H. B., Bates, C. R., Phillips, D. R., Simon, K. M., and Beckham, W. E., 1999, Detection and analysis of naturally fractured gas reservoirs: Multiazimuth seismic surveys in the Wind River basin, Wyoming: Geophysics, **64**, 1277–1292.

Hudson, J. A., 1980, Overall properties of a cracked solid: Math. Proc. Camb. Phil. Soc., **88**, 371–384.

——— 1981, Wave speeds and attenuation of elastic waves in material containing cracks: Geophys. J. Roy. Astr. Soc., **64**, 133–150.

Lines, L. R., and Treitel, S., 1984, Tutorial: A review of least-squares inversion and its application to geophysical problems: Geophys. Prosp., **32**, 159–186.

Lynn, H. B., Simon, K. M., Bates, C. R., and Van Dork, R., 1996, Azimuthal anisotropy in *P*-wave 3-D (multiazimuth) data: The Leading Edge, **15**, 923–928.

Lynn, H. B., Beckham, W. E., Simon, K. M., Bates, C. R., Layman, M., and Jones, M., 1999, *P*-wave and *S*-wave azimuthal anisotropy at a naturally fractured gas reservoir, Bluebell-Altamont field, Utah: Geophysics, **64**, 1293–1311.

MacBeth, C., and Lynn, H. B., 2000, Applied seismic anisotropy: Theory, background, and field studies: Soc. Expl. Geophys.

Nelson, R. A., 1985, Geologic analysis of naturally fractured reservoirs: Gulf Publ. Co.

Rüger, A., 1997, *P*-wave reflection coefficients for transversely isotropic models with vertical and horizontal axis of simmetry: Geophysics, **62**, 713–722.

Schoenberg, M., 1983, Reflection of elastic waves from periodically stratified media with interfacial slip: Geophys. Prosp., **31**, 265–292.

Schoenberg, M., and Sayers, C., 1995, Seismic anisotropy of fractured rock: Geophysics, **60**, 204–211.

Wapenaar, C. P. A., Peels, G., Budejicky, V., and Berkhout, A., 1989, Inverse extrapolation of primary seismic waves: Geophysics, **54**, 853–863.

Wu, R. S., and Toksöz, M. N., 1987, Diffraction tomography and multisource holography applied to seismic imaging: Geophysics, **52**, 11–25.

Zillmer, M., Gajewski, D., and Kashtan, B. M., 1998, Anisotropic reflection coefficients for a weak-contrast interface: Geophys. J. Internat., **132**, 159–166.

APPENDIX A
CALCULATION OF $\cos\theta$

Figure A-1 shows the Ω plane of Figure 4; θ is the angle between the incident wavenumber vector $\mathbf{k}_i$ and the medium wavenumber vector $\mathbf{k}_m$. The scalar product of these two vectors is

$$-\mathbf{k}_i \cdot \mathbf{k}_m = |\mathbf{k}_i||\mathbf{k}_m| \cos\theta. \tag{A-1}$$

Substituting the expressions for $\mathbf{k}_i$ and $\mathbf{k}_m$ into the equation (A-1), we obtain

$$\cos\theta = -\frac{k_{ix}(k_{rx}-k_{ix}) + k_{iy}(k_{ry}-k_{iy}) + k_{iz}(k_{rz}-k_{iz})}{\left(\frac{\omega}{v_i}\right)\sqrt{k_{mx}^2 + k_{my}^2 + k_{mz}^2}}, \tag{A-2}$$

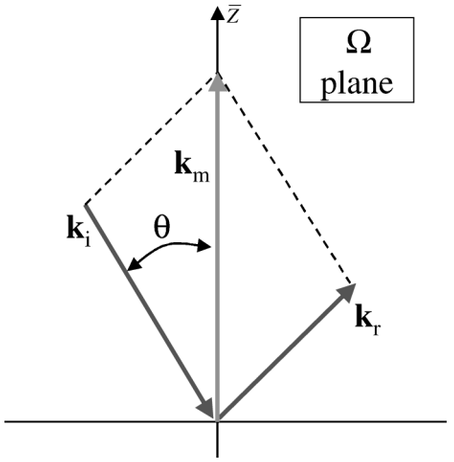

FIG. A-1. Plane Ω of Figure 4.

which simplifies to

$$\cos\theta = \frac{\left(\frac{\omega}{v_i}\right)^2 - k_{ix}k_{rx} - k_{iy}k_{ry} - k_{iz}k_{rz}}{\left(\frac{\omega}{v_i}\right)\sqrt{k_{mx}^2 + k_{my}^2 + k_{mz}^2}}. \tag{A-3}$$

Using

$$\begin{aligned} -k_{ix}k_{rx} &= \frac{(k_{rx}-k_{ix})^2 - k_{rx}^2 - k_{ix}^2}{2}, \\ -k_{iy}k_{ry} &= \frac{(k_{ry}-k_{iy})^2 - k_{ry}^2 - k_{iy}^2}{2}, \\ -k_{iz}k_{rz} &= \frac{(k_{rz}-k_{iz})^2 - k_{rz}^2 - k_{iz}^2}{2} \end{aligned} \tag{A-4}$$

with

$$\begin{aligned} k_{ix}^2 + k_{iy}^2 + k_{iz}^2 &= (\omega/v_i)^2, \\ k_{rx}^2 + k_{ry}^2 + k_{rz}^2 &= (\omega/v_r)^2, \end{aligned} \tag{A-5}$$

and remembering that

$$\begin{aligned} k_{mx}^2 &= (k_{rx}-k_{ix})^2, \\ k_{my}^2 &= (k_{ry}-k_{iy})^2, \\ k_{mz}^2 &= (k_{rz}-k_{iz})^2, \end{aligned} \tag{A-6}$$

after some algebra, equation (A-3) becomes

$$\cos\theta = \frac{\left(\frac{\omega}{v_i}\right)^2 - \left(\frac{\omega}{v_r}\right)^2 + k_{mx}^2 + k_{my}^2 + k_{mz}^2}{2\left(\frac{\omega}{v_i}\right)\sqrt{k_{mx}^2 + k_{my}^2 + k_{mz}^2}}, \tag{A-7}$$

which gives the relation between θ, the medium wavenumber components (k_{mx}, k_{my}, k_{mz}), and the angular frequency ω.

Equation (A-7) is invertible with respect to ω. For a given medium wavenumber $\mathbf{k}_m$, a variation in θ produces a variation in ω.

APPENDIX B
CALCULATION OF $\tan\phi$

The calculation of the azimuthal angle ϕ is a bit more complicated than that of the incident angle θ. Figure B-1 shows the plane Γ, perpendicular to the model vector $\mathbf{k}_m$, highlighted in Figure 4, where ϕ is the angle in the plane Γ between the projection of the vector $\mathbf{k}_i$ and the normal to the fracture $\mathbf{n}_f$. The components of $\mathbf{k}_i$ and $\mathbf{n}_f$ in the $(\bar{x}, \bar{y}, \bar{z})$ coordinate system are

$$\bar{k}_{ix} = \frac{k_{ix}k_{my} - k_{iy}k_{mx}}{\sqrt{k_{mx}^2 + k_{my}^2}},$$

$$\bar{k}_{iy} = \frac{k_{mz}(k_{ix}k_{mx} + k_{iy}k_{my})}{\sqrt{k_{mx}^2 + k_{my}^2}\sqrt{k_{mx}^2 + k_{my}^2 + k_{mz}^2}} - \frac{\sqrt{k_{mx}^2 + k_{my}^2}\sqrt{(\omega/v_i)^2 - k_{ix}^2 - k_{iy}^2}}{\sqrt{k_{mx}^2 + k_{my}^2 + k_{mz}^2}}, \tag{B-1}$$

$$\bar{k}_{iz} = \frac{k_{ix}k_{mx} + k_{iy}k_{my}}{\sqrt{k_{mx}^2 + k_{my}^2 + k_{mz}^2}} + \frac{k_{mz}\sqrt{(\omega/v_i)^2 - k_{ix}^2 - k_{iy}^2}}{\sqrt{k_{mx}^2 + k_{my}^2 + k_{mz}^2}}$$

and

$$\bar{n}_{fx} = \frac{n_{fx}k_{my} - n_{fy}k_{mx}}{\sqrt{k_{mx}^2 + k_{my}^2}},$$

$$\bar{n}_{fy} = \frac{k_{mz}(n_{fx}k_{mx} + n_{fy}k_{my})}{\sqrt{k_{mx}^2 + k_{my}^2}\sqrt{k_{mx}^2 + k_{my}^2 + k_{mz}^2}}$$

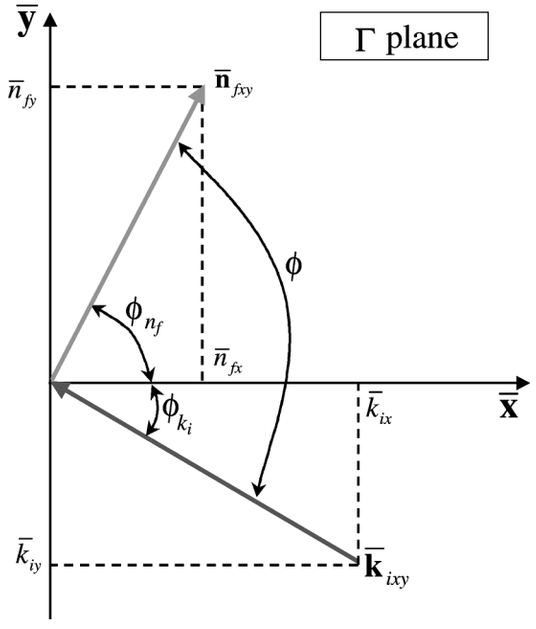

FIG. B-1. Plane Γ of Figure 4.

$$- \frac{n_{fz}\sqrt{k_{mx}^2 + k_{my}^2}}{\sqrt{k_{mx}^2 + k_{my}^2 + k_{mz}^2}}, \tag{B-2}$$

$$\bar{n}_{fz} = \frac{n_{fx}k_{mx} + n_{fy}k_{my}}{\sqrt{k_{mx}^2 + k_{my}^2 + k_{mz}^2}} + \frac{k_{mz}n_{fz}}{\sqrt{k_{mx}^2 + k_{my}^2 + k_{mz}^2}}.$$

From Figure B-1, the angles ϕ_{k_i} and ϕ_{n_f} can be written as

$$\phi_{k_i} = \arctan\left[\frac{\bar{k}_{iy}}{\bar{k}_{ix}}\right]$$

$$= \arctan \tag{B-3}$$

$$\times \left[\frac{k_{mz}(k_{mx}k_{ix} + k_{my}k_{iy}) - \left(k_{mx}^2 + k_{my}^2\right)\sqrt{(\omega/v_i)^2 - k_{ix}^2 - k_{iy}^2}}{(k_{my}k_{ix} - k_{mx}k_{iy})\sqrt{k_{mx}^2 + k_{my}^2 + k_{my}^2}}\right]$$

and

$$\phi_{n_f} = \arctan\left[\frac{\bar{n}_{fy}}{\bar{n}_{fx}}\right]$$

$$= \arctan\left[\frac{k_{mz}(k_{mx}n_{fx} + k_{my}n_{fy}) - \left(k_{mx}^2 + k_{my}^2\right)n_{fz}}{(k_{my}n_{fx} - k_{mx}n_{fy})\sqrt{k_{mx}^2 + k_{my}^2 + k_{my}^2}}\right]. \tag{B-4}$$

The angle ϕ between vectors $\bar{k}_{ixy}$ and $\bar{n}_{fxy}$ is the difference between the angles ϕ_{k_i} and ϕ_{n_f}:

$$\phi = \phi_{n_f} - \phi_{k_i} = \arctan\left[\frac{\bar{n}_{fy}}{\bar{n}_{fx}}\right] - \arctan\left[\frac{\bar{k}_{iy}}{\bar{k}_{ix}}\right]. \tag{B-5}$$